X-ray-excited optical luminescence of protein crystals: a new tool for studying radiation damage during diffraction data collection

Robin L. Owen,[a]* Briony A. Yorke[b] and Arwen R. Pearson[b]*

[a]Diamond Light Source, Harwell Science and Innovation Campus, Didcot, Oxfordshire OX11 0DE, England, and [b]Astbury Centre for Structural Molecular Biology, University of Leeds, Leeds LS2 9JT, England

Correspondence e-mail: robin.owen@diamond.ac.uk, a.r.pearson@leeds.ac.uk

During X-ray irradiation protein crystals radiate energy in the form of small amounts of visible light. This is known as X-ray-excited optical luminescence (XEOL). The XEOL of several proteins and their constituent amino acids has been characterized using the microspectrophotometers at the Swiss Light Source and Diamond Light Source. XEOL arises primarily from aromatic amino acids, but the effects of local environment and quenching within a crystal mean that the XEOL spectrum of a crystal is not the simple sum of the spectra of its constituent parts. Upon repeated exposure to X-rays XEOL spectra decay non-uniformly, suggesting that XEOL is sensitive to site-specific radiation damage. However, rates of XEOL decay were found not to correlate to decays in diffracting power, making XEOL of limited use as a metric for radiation damage to protein crystals.

1. Introduction

Macromolecular crystallography (MX) is a powerful tool for understanding the structure and function of macromolecules. However, the information that can be obtained from a macromolecular structure is limited by a combination of factors. These include the maximum resolution of the data that can be obtained, which is linked to the ease with which electronically distinct but structurally similar states can be distinguished in the electron-density map, and the progressive radiation damage to the structure that occurs during the diffraction experiment (Garman, 2010). One approach to dealing with these limitations has been the use of an increasing array of complementary measurements that can be recorded in concert with the diffraction experiment (Pearson & Owen, 2009). These provide additional local structural information that can be combined with the X-ray diffraction data to produce a more accurate description of the molecular structure and include UV–Vis absorption, fluorescence, infrared and Raman spectroscopies as well as EXAFS, XANES and SAXS/WAXS (Pearson & Owen, 2009; Grant et al., 2011; Sage et al., 2011).

Here, we investigate a relatively unexplored phenomenon in macromolecular crystallography: the glowing, or luminescence, of macromolecular crystals upon X-ray irradiation. Luminescence during irradiation is a phenomenon that is common to all molecules and that occurs during all X-ray data collections, in which crystals emit visible light during, and for a short time subsequent to, X-ray exposure. This is known as X-ray-excited optical luminescence (XEOL). XEOL occurs when photoelectric effect-induced excited states decay via a

visible electronic transition. In macromolecules this is most commonly de-excitation of the lowest lying singlet and triplet levels in the π-electron system of the aromatic ring. XEOL intensity is proportional to the intensity of the incident X-rays and the form of the spectra are a function of both the atomic number of the constituent elements within the sample and the local chemical structure (Rogalev & Goulon, 2002). XEOL is commonly used in the physical and material sciences to provide information on elemental composition, coordination geometry and electronic properties and is the basis of scintillator methods of X-ray detection (Rogalev & Goulon, 2002). Light atoms ($Z \leq 16$) emit a very weak XEOL signal and therefore it is rarely observed in macromolecular samples. Early work estimated luminescence yields from dried powders of both amino acids and proteins, and also investigated the effect of solvent quenching on spectra (Carter et al., 1965; Nelson et al., 1967; Nummedal & Steen, 1969). More recently, tuneable soft X-rays have been used to probe the optical properties of proteins conjugated to an extrinsic fluorophore (Kim et al., 2004).

An interesting application of XEOL in materials science has been the study of the mechanisms of radiolysis (Holroyd et al., 1993; Brocklehurst, 1993). Recently, McGeehan and coworkers reported the measurement of XEOL from a trypsin crystal using the online single-crystal spectrometer at ID14-2, ESRF (McGeehan et al., 2009). Interestingly, this signal bleached with increasing X-ray dose. This raises the intriguing possibility that XEOL studies of macromolecular crystals may shed light on the specific changes that occur during X-ray illumination. Although the initial physical processes (direct and secondary ionizations, generation of solvated electrons and radical species) and the resultant effects of radiation damage (redox-centre reduction, disulfide-bond cleavage, decarboxylation etc.) are well known (Garman, 2010), the chemistry of radiation damage in a macromolecular sample remains poorly defined. Radiation damage is the major limitation on the resolution and quality of diffraction data that can be obtained from a macromolecular crystal. Therefore, understanding how, why, when and where damage processes occur is key to the design of data-collection and processing protocols that enable us to determine undamaged and biologically relevant structures.

Here, we report further characterization of macromolecular XEOL using several proteins. We identify the nature of the contributing amino acids and investigate how XEOL spectra change with increasing absorbed dose.

2. Experimental methods

2.1. Sample preparation and data collection

2.1.1. Measurement of XEOL spectra. The SLS on-axis microspectrophotometer (Owen et al., 2009) was used on beamline X10SA of the Swiss Light Source, Paul Scherrer Institut, Villigen, Switzerland without modification. Luminescence spectra were collected in a 180° scattering geometry. A grating with 150 lines per millimetre blazed at 300 nm was

used for all data collections, resulting in a spectral resolution of <1 nm. Owing to the weak nature of the effect, care was taken to eliminate all ambient lighting from the experimental hutch. The focal spot size at the sample was ∼60 µm in diameter. XEOL spectra were recorded between 300 and 900 nm (Shamrock 303i spectrograph, Newton CCD, Andor Technology). All SLS XEOL and diffraction data were collected at an X-ray energy of 12.4 keV and with an X-ray beam size of 50×50 µm (1×10^{12} photons s^{-1}). As the X-ray and spectrometer shutters could not be synchronized at the time of the experiments, a spectrograph accumulation time of half that of X-ray exposure was used to ensure the X-ray shutter was completely open for at least one spectral accumulation. XEOL data were also collected on beamline I24 at Diamond Light Source at an X-ray energy of 12.68 keV and with the beam size at the sample defocused to 30×30 µm (1×10^{12} photons s^{-1}). In this case an off-axis geometry and reflective lenses (Royant et al., 2007) were used. The optical focal spot size at the sample was ∼60 µm in diameter. Luminescence spectra were collected between 200 and 750 nm (Shamrock 303i spectrograph, Newton CCD, Andor Technology).

2.1.2. Protein crystals and diffraction data collection. Hen egg-white lysozyme (HEWL), thermolysin and equine spleen apoferritin and holoferritin were obtained from Sigma and were crystallized using standard techniques without further purification. Crystallization conditions and fractional aromatic amino-acid compositions of all samples used are summarized in Table 1. Crystals of Escherichia coli N-acetyl-D-neuraminic acid lyase (NAL; Campeotto et al., 2009) were kindly supplied by Ivan Campeotto (University of Leeds). The crystals of apoferritin and holoferritin were grown in identical crystallization conditions and were cryoprotected in mother liquor containing 40% glycerol; the crystallization conditions of other crystals were such that no additional cryoprotectant was required. All data were collected with protein crystals held at 100 K. SLS diffraction data were recorded using a MAR 225 detector. For each sample, the same 1° oscillation image was collected repeatedly in order to monitor changes in the integrated intensity of the same reflections with increasing X-ray dose.

2.1.3. Amino acids. Crystalline chromatographically homogenous amino acids were obtained from BDL (Amino Acid Reference Collection for Paper and Thin Layer Chromatography). Amino-acid crystals (DL-alanine, L-arginine, L-cysteine, L-cystine, L-glutamate, L-histidine, L-leucine, DL-methionine, DL-phenylalanine, L-proline, DL-tryptophan and L-tyrosine) larger than or equal to the beam size were mounted in a nylon loop, suspended in a thin film of dimethylsulfoxide (DMSO) and flash-cooled to 100 K in a nitrogen cryostream. XEOL spectra were accumulated over 10 s. For each amino acid tested an initial spectrum was recorded with the X-ray shutter closed, followed by a series of spectra with the X-ray shutter open.

2.1.4. Common cryoprotectants. In order to establish whether the sole contribution to the XEOL spectra was from the amino-acid or protein crystals, XEOL data were collected

Table 1
Crystallization conditions and fractional aromatic amino-acid compositions of the crystals used.

| Crystal | Crystallization conditions | Amino-acid composition (No.) | | | | No. of disulfides |
		His	Phe	Trp	Tyr	
Ferritin	0.6 M (NH$_4$)$_2$SO$_4$, 10 mM CdSO$_4$	3.4% (6)	1.1% (2)	0.57% (1)	3.4% (6)	0
HEWL	7%(w/v) NaCl, 0.1 M sodium acetate pH 4.7, 20% ethylene glycol	0.78% (1)	1.6% (2)	4.7% (6)	2.3% (3)	4
NAL	100 mM Tris–HCl pH 8.2, 200 mM ammonium acetate, 18% PEG 3350	3.6% (11)	3.6% (11)	0.33% (1)	4.3% (13)	0
Thermolysin	50 mM MES, 1 M NaCl, 45%(v/v) DMSO	2.5% (8)	2.5% (8)	0.94% (3)	8.9% (28)	0
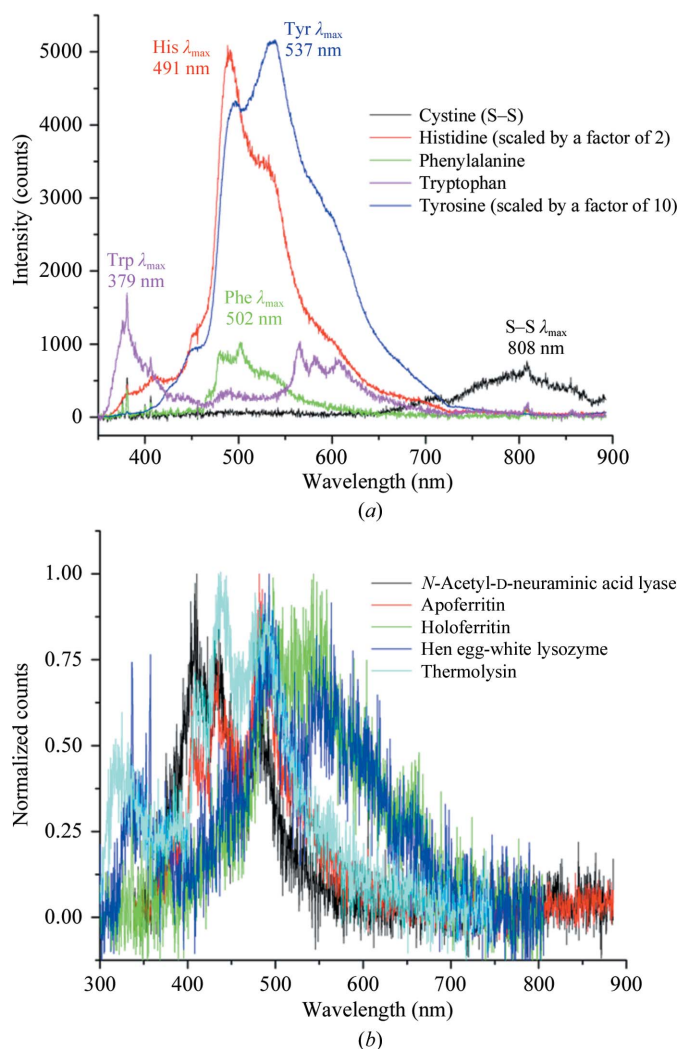
Figure 1
(a) XEOL spectra from crystalline amino acids in DMSO. The histidine and tyrosine spectra have been scaled down by factors of two and ten, respectively, in order to allow direct comparison of spectra from all of the samples. (b) Raw XEOL spectra from crystalline proteins highlighting the magnitude of the effect with respect to noise and the need to filter high-frequency noise prior to data analysis. Thermolysin data were collected on I24 at DLS; all other data were collected on X10SA at SLS.

from thin films of cryoprotectants. Thin films of glycerol, 2-methyl-2,4-pentanediol (MPD), DMSO and paraffin oil were mounted in nylon loops and cooled to 100 K in a nitrogen cryostream. XEOL spectra were accumulated over 5 s. An initial spectrum was recorded with the X-ray shutter closed, followed by a series of spectra with the X-ray shutter open.

2.2. Data processing

2.2.1. X-ray diffraction data. X-ray diffraction data were analysed using *LABELIT* (Zhang *et al.*, 2006; Sauter & Poon, 2010). Using *DISTL*, the integrated signal strength given in pixel-ADC units above local background of all Bragg candidates was calculated on a per-image basis. This was defined as the diffracting power of the crystal, allowing rapid determination of the diffracting power as a function of time. In order to facilitate comparison of the decay in diffracting power and XEOL of different crystals, the diffracting power was normalized such that the diffracting power of the first image of a data set was 1.00. The dose absorbed by the samples was calculated using *RADDOSE* (Paithankar *et al.*, 2009). For holoferritin dose calculations, the iron content was assumed to be 1760 Fe atoms per 24-mer (Owen *et al.*, 2006). For both the X10SA and I24 experiments the crystals used were larger than the beam size. As crystals were rotated only 1° during data collection, the beam size could be used to calculate the absorbed dose.

2.2.2. XEOL. As XEOL is such a weak effect, the recorded spectra from a short (<1 s) X-ray exposure are extremely noisy (Fig. 1b). Longer X-ray exposure and accumulation times such as those used in §2.1.3 to improve the signal-to-noise ratio were determined to be undesirable for two reasons. Firstly, the XEOL signal decays non-uniformly on these timescales and, secondly, such exposure times are not consistent with typical X-ray diffraction data-acquisition times in MX. In order to facilitate the extraction of decay rates and the determination of λ_{max} values, raw XEOL spectra were passed through a low-pass FFT filter (0.09 Hz) to remove high-frequency noise. This treatment produced clear and usable spectra (Fig. 2) for exposures as short as 0.5 s from which the temporal evolution of spectral features could be evaluated. Savitzky–Golay and moving point average smoothing methods were also tested, but did not yield satisfactory results. The total luminescence yield at each time point was determined by integration of the smoothed XEOL spectra between 300 and 805 nm.

3. Results and discussion

Spectra collected from individual crystalline amino acids suspended in DMSO showed XEOL to arise predominantly from aromatic amino acids (Fig. 1a). The λ_{max} of the aromatic amino acids varied between 380 and 537 nm. No XEOL was

observed between 300 and 900 nm from any other amino acid tested apart from cystine. Cystine yielded a weak XEOL signal with a λ_{max} of 808 nm that is likely to arise from the disulfide bond. The spectral shapes observed are broadly consistent with previously recorded XEOL data for tyrosine, tryptophan and phenylalanine powders and for tryptophan dissolved in 1:1 water:ethylene glycol (Carter *et al.*, 1965; Steen, 1967, 1968; Nelson *et al.*, 1967; Nummedal & Steen, 1969). The XEOL spectra bleached after continued exposure to X-rays, as previously observed in other inorganic systems (Rogalev & Goulon, 2002). The spectra were not observed to change as a function of crystal orientation. There were some differences between the λ_{max} values observed here and those in the early literature. These are likely to be a consequence of a combi-nation of differences in solvent polarity, the flux density of incident X-rays and the temperature and state of the samples (powder, solution or crystalline).

Glycerol, MPD and DMSO did not exhibit XEOL, consistent with their chemical structures. Paraffin oil demonstrated a broad and strong XEOL signal across the same wavelength range as proteins and is therefore an unsuitable cryoprotectant for use in XEOL studies.

XEOL spectra were recorded from HEWL, apoferritin and holoferritin, NAL and thermolysin. These complex spectra showed distinct features for each protein (Figs. 2a and 2b); the spectra did not show any change as a function of crystal
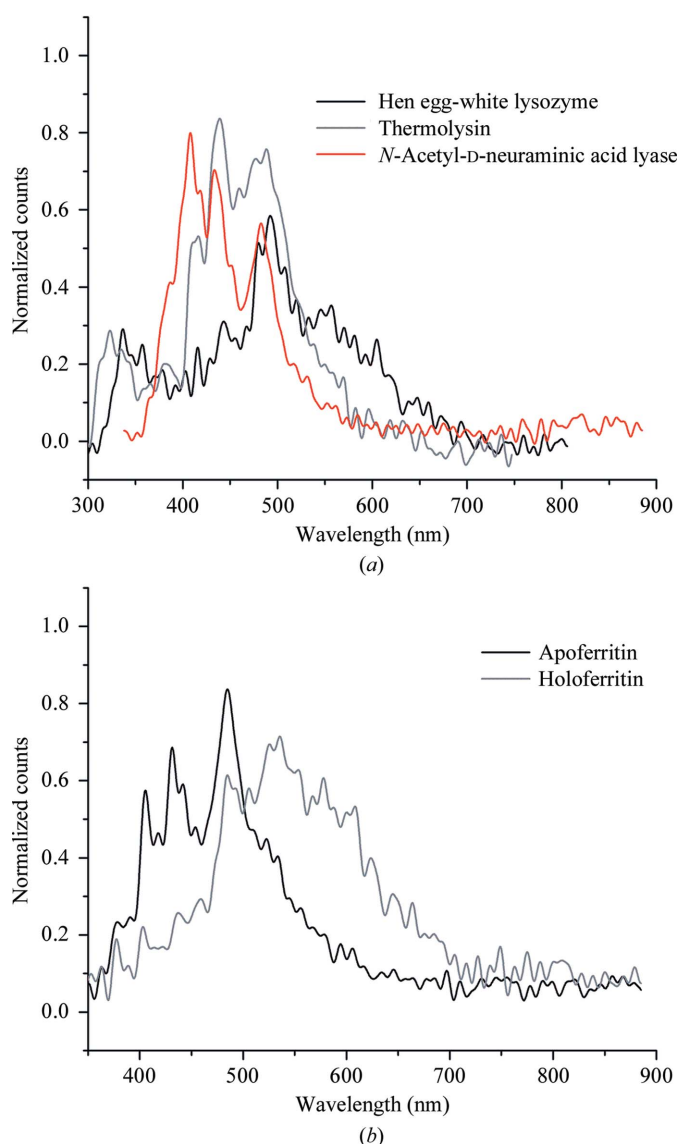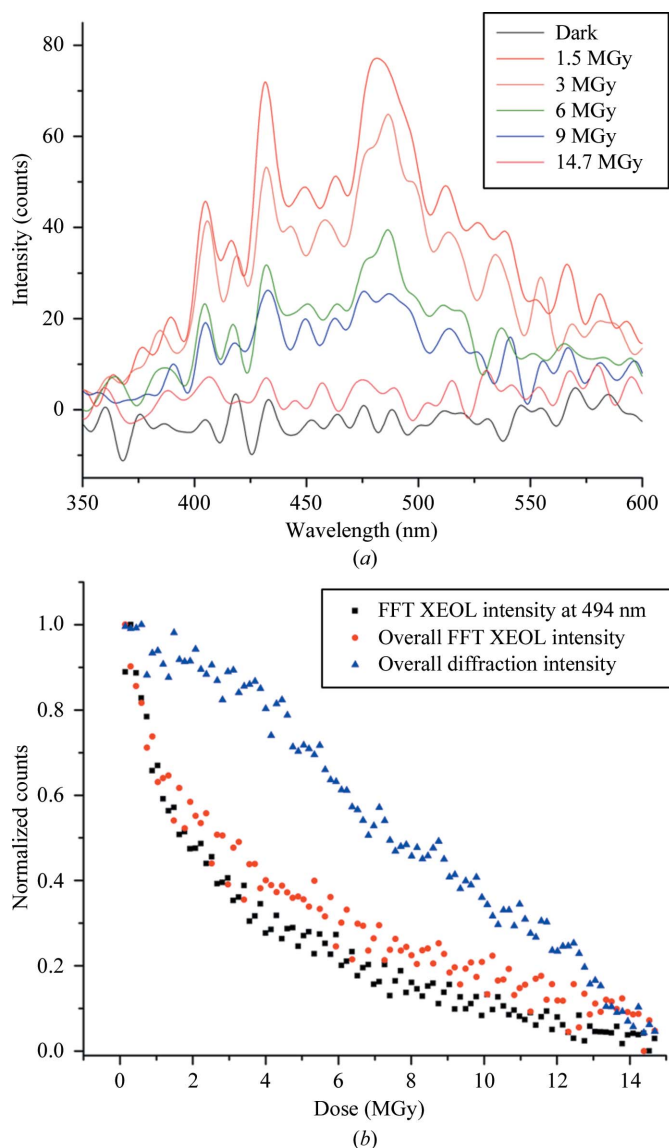

Figure 2
(a) The XEOL spectra from lysozyme, thermolysin and NAL shown in Fig. 1(b) after passage through a low-pass FFT filter. Distinct features and differences between spectra from different samples can now be easily observed. (b) Apoferritin and holoferritin display markedly different XEOL, with luminescence at wavelengths greater than 500 nm reduced in holoferritin.

Figure 3
(a) Decay of apoferritin XEOL spectra as a function of absorbed dose and (b) the concomitant decay of diffracting power and luminescence (both overall and at the peak XEOL wavelength) of the same apoferritin crystal as a function of absorbed dose. XEOL decay is tracked both as a function of the normalized intensity at 494 nm (maximum of initial spectra; black squares) and the overall luminescence yield (as defined in §2.2.2; red circles). The decay in normalized diffracting power is also shown (as defined in §2.2.1; blue triangles). All data were collected on X10SA at SLS.

orientation. Comparison of the protein XEOL with the XEOL of individual amino acids and consideration of the amino-acid composition of each protein indicated that the protein XEOL is not the simple sum of the luminescence of its constituent amino acids. The λ_{max} of the protein XEOL spectra are also red-shifted compared with those of the amino acids in DMSO. These observations indicate that XEOL, like fluorescence, is sensitive to local environment (*i.e.* polarity and nonradiative transfer) and that the luminescence of specific amino acids is quenched or altered when incorporated into a protein. This is particularly evident when the XEOL spectra of apoferritin and holoferritin are compared, where there is both an overall red shift and a change in spectral shape. This possibly arises from a combination of the increased protein dielectric constant and both radiative and nonradiative transfer in the presence of the amorphous iron core of holoferritin.

XEOL spectra were observed to rapidly decay during exposure to X-rays. Longer accumulation times resulted in smoother spectra, but in order to achieve a higher time resolution shorter exposure times were used in conjunction with FFT smoothing. This decay is shown for an apoferritin crystal in Fig. 3(*a*). In order to establish whether this decay is correlated to a decay in diffracting power, diffraction data and XEOL spectra were collected simultaneously from apoferritin and holoferritin, HEWL and NAL crystals. The decay of both the total luminescence yield and the peak counts from an apoferritin crystal are compared with the decay in diffracting power in Fig. 3(*b*). In this case XEOL follows a single exponential decay. Despite the comparable decay rates observed in this example, further investigation using several proteins showed that XEOL decay correlated poorly with decay in diffracting power. A wide range of XEOL decay rates were observed, even between crystals of the same type. In addition,
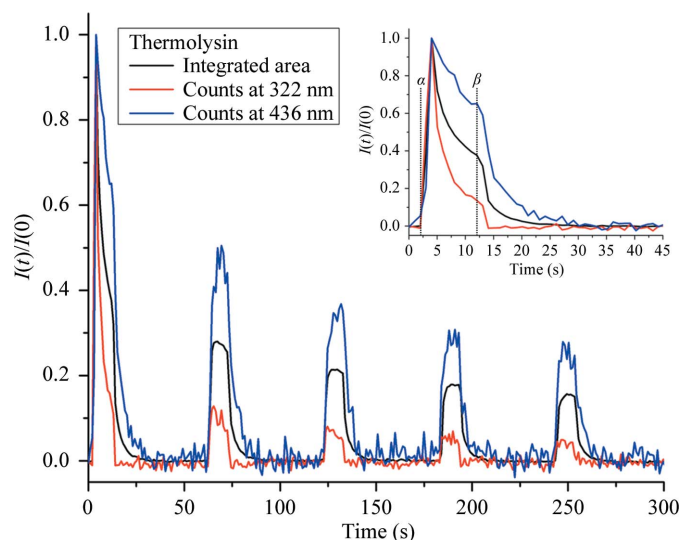

Figure 4
Decay in luminescence of a thermolysin crystal as a function of time. XEOL spectra show differential rates of decay as a function of wavelength and a lack of recovery between X-ray pulses. The cumulative dose absorbed by the crystal per pulse is 3.6 MGy. The inset shows an expanded view of the first pulse; the X-ray shutter is opened at $t = \alpha$ and closed at $t = \beta$. All data were collected on I24 at DLS.

XEOL was observed to not always follow a single exponential decay, with some crystals better described by a double exponential decay. During these experiments XEOL and diffraction data were collected with the simplest possible experiment design: each diffraction image was collected over the same repeated angular range. The lack of correlation and consistency observed with this simplified experimental setup suggests that XEOL is not (with currently available instrumentation) a reliable metric for following radiation damage.

Bleaching of fluorescence is usually associated with the irreversible destruction of the fluorophore (Adam *et al.*, 2009). In order to determine whether a similar irreversible process occurs during the bleaching of the XEOL signal during X-ray exposure, we collected a series of thermolysin XEOL spectra using a sequence of X-ray pulses spaced such that the XEOL signal could completely decay before the next X-ray pulse occurred (Fig. 4). These data showed several interesting features. Firstly, the XEOL signal does not recover even after extended delays (50 s) between each X-ray pulse. Instead, a progressive bleaching is observed consistent with destruction of the luminescent moieties. Secondly, spectral features with differing λ_{max} showed a clear difference both in XEOL lifetime after the X-ray shutter closed and in bleaching rate. Previously, almost complete recovery of fluorescence spectra has been observed for crystals subjected to low doses (<1 MGy; Adam *et al.*, 2009). The lack of XEOL recovery in this study can be attributed to the large absorbed dose per pulse (~3.6 MGy), meaning that even if intermediates only infrequently convert to a permanently damaged state the damaged state becomes highly populated. The non-uniform decay of XEOL spectra suggests that XEOL reflects differential damage rates at distinct sites within the protein. It has been shown that different amino acids are damaged at different rates during X-ray irradiation depending on the type of side chain and its local environment (Garman, 2010). This is consistent with the wavelength-dependent luminescence decay observed here. This non-uniform decay suggests that further characterization and understanding of macromolecular XEOL will help to reveal how individual amino acids respond to X-ray irradiation and allow us to develop a more complete model of the progression of radiation damage in macromolecules.

4. Conclusions

Despite being a relatively weak phenomenon for protein crystals, XEOL could easily be recorded using the microspectrophotometers at SLS and DLS. XEOL in proteins arises primarily from aromatic amino acids, but the effects of local environment and quenching within crystals means that the spectra are not a simple sum of the spectra arising from the constituent parts of the crystals. Global rates of XEOL decay were found not to correlate to decays in diffracting power, making XEOL of limited use as a metric for radiation damage to protein crystals. However, the decay of XEOL spectra is non-uniform, suggesting that XEOL is sensitive to site-specific radiation damage of aromatic amino acids and may be of use

in developing a better understanding of the mechanisms of radiation damage in MX.

References

Adam, V., Carpentier, P., Violot, S., Lelimousin, M., Darnault, C., Nienhaus, G. U. & Bourgeois, D. (2009). *J. Am. Chem. Soc.* **131**, 18063–18065.

Brocklehurst, B. (1993). *Chem. Phys. Lett.* **211**, 31–35.

Campeotto, I., Carr, S. B., Trinh, C. H., Nelson, A. S., Berry, A., Phillips, S. E. V. & Pearson, A. R. (2009). *Acta Cryst.* F**65**, 1088–1090.

Carter, J. G., Nelson, D. R. & Augenstein, L. G. (1965). *Arch. Biochem. Biophys.* **111**, 270–282.

Garman, E. F. (2010). *Acta Cryst.* D**66**, 339–351.

Grant, T. D., Luft, J. R., Wolfley, J. R., Tsuruta, H., Martel, A., Montelione, G. T. & Snell, E. H. (2011). *Biopolymers*, **95**, 517–530.

Holroyd, R. A., Preses, J. M. & Hanson, J. C. (1993). *Radiat. Res.* **135**, 312–314.

Kim, P.-S. G., Petersen, N. O., Sham, T. K. & Hu, Y. F. (2004). *Chem. Phys. Lett.* **392**, 44–49.

McGeehan, J., Ravelli, R. B. G., Murray, J. W., Owen, R. L., Cipriani, F., McSweeney, S., Weik, M. & Garman, E. F. (2009). *J. Synchrotron Rad.* **16**, 163–172.

Nelson, D. R., Carter, J. G., Birkhoff, R. D., Hamm, R. N. & Augenstein, L. G. (1967). *Radiat. Res.* **32**, 723–743.

Nummedal, D. & Steen, H. B. (1969). *Radiat. Res.* **39**, 241–251.

Owen, R. L., Pearson, A. R., Meents, A., Boehler, P., Thominet, V. & Schulze-Briese, C. (2009). *J. Synchrotron Rad.* **16**, 173–182.

Owen, R. L., Rudiño-Piñera, E. & Garman, E. F. (2006). *Proc. Natl Acad. Sci. USA*, **103**, 4912–4917.

Paithankar, K. S., Owen, R. L. & Garman, E. F. (2009). *J. Synchrotron Rad.* **16**, 152–162.

Pearson, A. R. & Owen, R. L. (2009). *Biochem. Soc. Trans.* **37**, 378–381.

Rogalev, A. & Goulon, J. (2002). *Chemical Applications of Synchrotron Radiation. Part II: X-ray Applications*, edited by T. K. Sham, pp. 707–760. River Edge: World Scientific.

Royant, A., Carpentier, P., Ohana, J., McGeehan, J., Paetzold, B., Noirclerc-Savoye, M., Vernède, X., Adam, V. & Bourgeois, D. (2007). *J. Appl. Cryst.* **40**, 1105–1112.

Sage, J. T., Zhang, Y., McGeehan, J., Ravelli, R. B. G., Weik, M. & van Thor, J. J. (2011). *Biochim. Biophys. Acta*, **1814**, 760–777.

Sauter, N. K. & Poon, B. K. (2010). *J. Appl. Cryst.* **43**, 611–616.

Steen, H. B. (1967). *Photochem. Photobiol.* **6**, 805–816.

Steen, H. B. (1968). *Photochem. Photobiol.* **8**, 47–51.

Zhang, Z., Sauter, N. K., van den Bedem, H., Snell, G. & Deacon, A. M. (2006). *J. Appl. Cryst.* **39**, 112–119.